A CALIBRATED SUBSTATION-BUILDING SIMULATOR FOR DISTRICT-HEATED RESIDENTIAL BUILDINGS AND EVALUATION OF CONTROL STRATEGIES

Christoffer Hansson and Gideon Mbiydzenyuy
Department of Information Technology
University of Borås
SE-501 90, Borås,
Sweden
email: {christoffer.hansson, gideon.mbiydzenyuy}@hb.se

KEYWORDS
Control systems, Energy, Model design, Lumped parameter, Differential equations

ABSTRACT

Evaluating control strategies directly in district-heated buildings is challenging because experimenting with control actions may compromise indoor comfort and operational reliability. This work develops and calibrates a dynamic grey-box simulator of a district-heated residential building using operational data. The simulator couples a thermal resistance–capacitance building model with heat-exchanger and hydronic radiator dynamics. Calibration and validation against historical data demonstrate the model's ability to approximate space-heating demand and provide a computationally efficient environment for comparative controller evaluation. Its use is demonstrated by comparing rule-based and proportional-integral control strategies and by establishing the feasibility of training and evaluating a reinforcement learning agent within the simulated environment, while providing a basis for future extension to building portfolios.

INTRODUCTION

The building sector accounts for approximately 27% of global final energy demand, while space heating (SH) and domestic hot water (DHW) account for nearly 70% of building energy use in advanced economies (International Energy Agency (2025)). With carbon neutrality targeted by 2050 (Rodrigues et al. (2026)), reducing building energy demand and associated emissions is therefore crucial. District heating (DH) has been identified as a promising solution for meeting future heating needs within this transition (Mathiesen et al. (2026)). A DH network distributes centrally produced hot water to connected buildings (see Fig. 1) which are equipped with a DH substation, providing an interface between the network, referred to as the primary side, and the building heating system, referred to as the secondary side. This coupled system exhibits complex transient dynamics driven by weather, occupancy, and heat demand. Consequently, control strategies are required to regulate heat delivery while maintaining indoor thermal comfort and limiting energy use. Traditionally, weather-compensation curves and proportional-integral (PI) controllers have been used to regulate building heating systems through supply-temperature control (Sleptsov et al. (2021)). More recently, supervisory control strategies, including model predictive control (Chaudhry et al. (2021)) and data-driven approaches (Zhang et al. (2023)), have been investigated as alternatives for improving operational performance. However, evaluating such strategies in operational systems requires accurate and computationally tractable models of the coupled substation–building dynamics. To address this, we develop a lightweight grey-box model of a district-heated residential building in Sweden and calibrate it using operational measurements. The model couples substation, hydronic radiator, and building-envelope dynamics while balancing computational efficiency and model fidelity. The resulting simulator is used to compare rule-based and PI control strategies, while reinforcement learning is included as a proof of concept to demonstrate the feasibility of training agents within the environment. Evaluation of the latter serves to verify learning and training practicality rather than to benchmark a fully optimized control strategy. These use cases provide a foundation for future portfolio-level applications and the continued development of reinforcement learning formulations within the simulator.

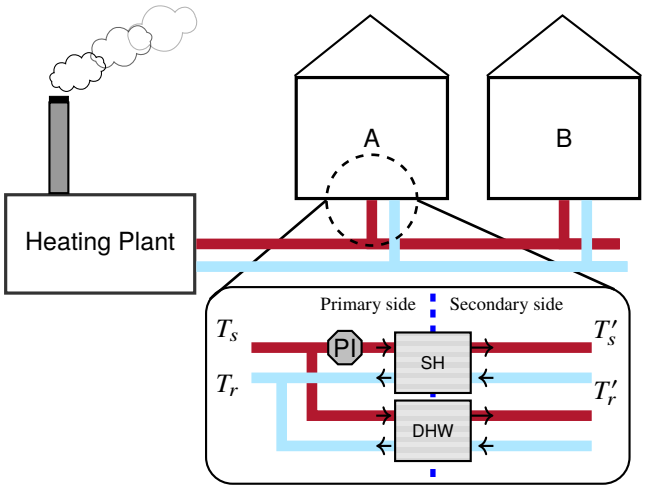

Figure 1: DH Network and a Building Substation

METHODOLOGY

Buildings in a DH network exert a heat load $\dot{Q}_L$, typically being a sum of space-heating, $\dot{Q}_{\mathrm{SH}}$, and DHW $\dot{Q}_{\mathrm{DHW}}$. The former is largely driven by heat losses through the building envelope while the latter is primarily dependent on occupant behavior (Lundström and Akander (2019)). In this work, we focus on modeling the SH component and the substation under consideration records only $\dot{Q}_L$. To formulate and calibrate a physical model for the SH demand, $\dot{Q}_{\mathrm{SH}}$ must be separated from $\dot{Q}_L$ and to this end, the heat demand associated with DHW is modeled as

$$\dot{Q}_{\mathrm{DHW}} = c_p \left(\dot{m}^{\mathrm{dhw}} \Delta T_{\mathrm{circ}} + \alpha \dot{m}^{\mathrm{dcw}} \Delta T_{\mathrm{DHW}} \right), \tag{1}$$

where c_p denotes the specific heat capacity of water, $\dot{m}^{\mathrm{dhw}}$ is the mass flow in the DHW circulation loop, and $\dot{m}^{\mathrm{dcw}}$ is the mass flow of domestic cold water (DCW). The term ΔT_{circ} represents the effective temperature difference associated with circulation losses, while ΔT_{DHW} is the temperature increase from DCW to DHW. The parameter α represents the fraction of DCW used for DHW preparation and is on average in the range $44 - 50\%$ (Lundström and Akander (2019)). A representative DHW temperature difference of $\Delta T_{\mathrm{DHW}} = 45°\mathrm{C}$ is assumed.

Substation and Hydronic Radiator Modeling

The first interaction between the DH substation and the secondary side occurs at a heat exchanger (see Fig. 1). Given a primary-side mass flow $\dot{m}$ and supply temperature T_s, the heat transfer is represented using an effective heat exchanger (Lienhard and Lienhard (2019))

$$\dot{Q}_{\mathrm{SH}} = \epsilon \cdot \min\left(\dot{m}, \dot{m}'\right) c_p \left(T_s - T_r'\right), \tag{2}$$

where $\epsilon \in [0, 1]$ denotes the heat exchanger effectiveness. Simultaneously, invoking energy balance across the exchanger allows us to write

$$\dot{Q}_{\mathrm{SH}} = \dot{m}' c_p \left(T_s' - T_r'\right), \tag{3}$$

where $\dot{m}', T_s', T_r'$ is the mass flow, supply and return temperature on the secondary-side, respectively. Heat is assumed to be delivered to the indoor air through an effective hydronic radiator system. The corresponding heat output is written as (Muniak (2017))

$$\dot{Q} = K \left(\Delta T_{\mathrm{LMTD}}\right)^n = K \left(\frac{T_s' - T_r'}{\ln\left(\frac{T_s' - T_i}{T_r' - T_i}\right)} \right)^n, \tag{4}$$

where K is the heat transfer coefficient of the radiator, n is the radiator exponent, ΔT_{LMTD} is the logarithmic mean temperature difference and T_i denotes the indoor air temperature. When coupling this to a building model driving a SH load, energy balance is enforced such that T_r' dictates that the heat transferred by Eq. (2) equals the heat emitted by Eq. (4). To close the simulation loop, the primary-side mass flow $\dot{m}$ passing through the heat exchanger is modeled by a PI-controlled actuator valve as shown in Fig. 1 (Sleptsov et al. (2021)). The controller tracks the deviation between a setpoint and measurements and adjusts its output by weighting the error by a proportional and integral part denoted K_p and K_i, respectively. A discretization of the PI controller with time step Δt is applied here.

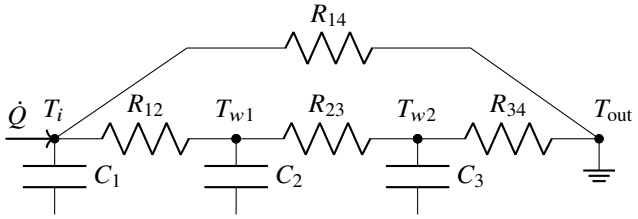

Figure 2: RC Representation of the Building Envelope

Building Grey-Box Modeling

Given substation meter data and limited knowledge of the building properties and occupancy, the grey-box modeling approach known as lumped thermal resistance–capacitance (RC) models (Boodi et al. (2022)) is adopted to represent the building thermal response. Specifically, a 4R3C structure (Wang et al. (2026)) as shown in Fig. 2 is chosen in order to balance model complexity while capturing multiple thermal timescales. To assess the impact of model complexity, a reduced 3R2C formulation is also considered, obtained by removing the state T_{w2} together with its associated capacitance C_3 and resistance R_{34}. Consequently, R_{23} then directly connects the remaining wall node to T_{out}. These models can be written in discrete state-space form

$$s_{t+1} = \mathcal{A} s_t + \mathcal{B} u_t, \tag{5}$$

where $\mathcal{A}, \mathcal{B}$ are the state update matrices, constructed using a zero-order hold assumption on the input vector $u = \left(\dot{Q}, T_{\mathrm{out}}\right)^\top$ wherein T_{out} is the outdoor temperature and $\dot{Q}$ is given by Eq. (4). Here, $s = \left(T_i, T_{w1}, T_{w2}\right)^\top$ is the state vector, representing one indoor state and two hidden wall states. Heat transfer through the walls are governed by R_{12}, R_{23}, R_{34} whereas R_{14} represents ventilation losses.

CALIBRATION & CASE STUDY

Calibration makes use of two datasets, hereafter denoted as D1 and D2, from a nine-story residential building comprising 35 apartments in Sweden. D1 provides high-resolution measurements over a limited time span, whereas D2 contains lower-resolution data spanning a substantially longer period. To ensure sufficient temporal coverage, the RC model is calibrated and validated using D2, while the heat-exchanger, radiator, and operational parameters are identified using D1. D2 contains approximately ten years of hourly measurements of primary-side mass flow, supply and return temperatures,

outdoor temperature and cold-water consumption. Due to the latter, the DHW preparation term in Eq. (1) is estimated and subtracted from the total heat consumption, while circulation losses cannot be explicitly separated. By comparing $\dot{Q}_L$ and $\dot{m}^{\mathrm{dcw}}$ during summer periods, for which $\dot{Q}_L \approx \dot{Q}_{\mathrm{DHW}}$, we estimate $\alpha \approx 43.85\%$. The resulting SH demand is used as input to the RC calibration, spanning the period January 2022 to January 2025, using a chronological 80/20 split for parameter estimation and validation.

D1 contains approximately one year of 10-minute measurements. In addition to most variables available in D2, it includes secondary-side supply and return temperatures, and the mean indoor temperature from 14 distributed sensors. Measurements of the DHW circulation circuit include $\dot{m}^{\mathrm{dhw}}$ and ΔT_{circ} but not $\dot{m}^{\mathrm{dcw}}$, thereby enabling estimation of the first term in Eq. (1) but not the second.

Substation Parameter Identification

Ordinary least squares is used to estimate ϵ in Eq. (2), with the fitted value constrained to the range $[0, 1]$. Data from the heating season is used, since estimating $\dot{m}'$ from Eq. (3) is less sensitive to measurement noise when $T'_s - T'_r$ is not close to zero. The parameters in Eq. (4) are estimated using nonlinear least squares. Since less than half of the apartments have indoor temperature sensors, a single aggregate radiator response is fitted using secondary-side temperatures and the mean indoor temperature $\bar{T}$ computed from the available sensors. Consequently, n is treated as a free effective parameter rather than being constrained to the typical range of 1.3–1.5 (Muniak (2017)). Its fitted value should not be interpreted as the physical exponent of an individual radiator, as the aggregate response also absorbs unmodeled pipe losses, spatial temperature variations, heterogeneous radiator characteristics, and measurement limitations. Finally, the mass flow controller parameters are selected by taking K_p directly from D1. Since the deployed PI controller operates at a higher update frequency than the simulator, K_i is scaled to the simulation time step of $\Delta t = 10$ min so that the integral contribution remains consistent with the original controller.

RC Parameter Optimization

Currently, the building operates under a proprietary control scheme that maintains the indoor temperature close to a prescribed setpoint. Consequently, indoor temperature reveals limited information on the building envelope dynamics and since D2 lacks these measurements, the model is calibrated using inferred space-heating demand rather than indoor temperature trajectories. The RC parameters θ are identified using differential evolution by minimizing the mean absolute error

$$\theta^* = \arg\min_{\theta} \left(N^{-1} \sum_{t=1}^{N} \left| \dot{Q}_{\mathrm{SH},t} - \hat{\dot{Q}}_{\mathrm{SH},t} \right| \right), \tag{6}$$

where N is the number of time steps used during calibration whereas $\dot{Q}_{\mathrm{SH},t}$ and $\hat{\dot{Q}}_{\mathrm{SH},t}$ denote measured and model-predicted demand, respectively. The latter is obtained by first propagating the RC model one time step with $\dot{Q} = 0$, yielding the next indoor state $T_{i,t+1}$, followed by computing the non-negative heating demand required to restore the indoor temperature setpoint $\hat{T}_i = 21°\mathrm{C}$.

CONTROL OBJECTIVE FORMULATION AND EVALUATION

One objective for a building operator is to reduce heat use without substantially compromising occupant comfort. As a demonstration case, we consider night setback, wherein heat supply is reduced during nighttime hours when occupants may be less sensitive to temporary comfort deviations (Dolinay and Vasek (2019)). Since night setback is not currently employed in the studied building, it provides a suitable test case for evaluating control strategies in the proposed simulator. Here, strategy performance is evaluated by recording the total consumption Q_{SH}, pumped water mass m_{tot}, peak mass flow $\dot{m}_{\mathrm{peak}}$, and comfort-violation severity S. Specifically,

$$S = \int_0^T (T_{\min}(t) - T_i(t))^+ + (T_i(t) - T_{\max}(t))^+ \, dt, \tag{7}$$

where $(\cdot)^+ = \max(\cdot, 0)$ denotes the positive part of the argument and $[T_{\min}(t), T_{\max}(t)]$ is the comfort temperature band being $[20.5, 21.5]°\mathrm{C}$ during daytime hours (06:00–22:00) and $[20.0, 21.5]°\mathrm{C}$ during nighttime hours. Concretely, all control approaches modify the setpoint value of T'_s:

$$\hat{T}'_s = f\,(T_{\mathrm{out}}) + g\,\left(T_i - \hat{T}_i\right) + \Delta\hat{T}'_s, \tag{8}$$

where $f(\cdot)$ and $g(\cdot)$ are the weather-compensation (WC) and indoor-compensation (IC) curves, respectively, identified from D1. As a refinement to these rule-based functions, a PI controller is used to generate the bounded trim $\Delta\hat{T}'_s \in [-10, 10]°\mathrm{C}$ from the indoor-temperature tracking error. The controller parameters are reported in Table 1, chosen to provide stable responsiveness in simulations.

Table 1: Identified and Calibrated Model Parameters

$R_{14} = 0.5, R_{12} = 0.03, R_{23} = 0.03, R_{34} = 92.94$ [KkW^{-1}]
$C_1 = 80.66, C_2 = 480.72, C_3 = 814.43$ [kWh K^{-1}]
$\epsilon = 1, n = 0.71, K = 7.39$ [kW K^{-n}]
$K_p = 1.67$ [%/K], $K_i = 1.5$ [%/(K · h)] (Mass flow cont.)
$K_p = 7, K_i = 1.25$ [1/h] (Setpoint trim cont.)

Reinforcement Learning

To demonstrate the simulator's applicability to learning-based control, a Soft Actor-Critic (SAC) agent (Haarnoja et al. (2018)) is trained to adjust $\Delta\hat{T}'_s$ via the agent action a_t. The

Table 2: Comparison of Control Approaches for Night Setbacks

Approach	**Setpoint** [°C]	Q_{SH} **[MWh]**	m_{tot} **[tons]**	$\dot{m}_{\mathrm{peak}}$ **[kg/h]**	S [°C-days]
WC	–	67.06	1166.83	1123.93	61.70
WC + IC	21.0	59.02	967.78	1001.47	1.05
WC + IC + PI-Trim	21.0	58.48	995.97	1238.29	2.04
WC + IC	20.8	58.42	951.33	992.68	1.59
WC + IC + PI-Trim	20.8	57.86	973.79	1233.17	2.46
WC + IC	20.6	57.84	935.07	986.98	2.59
WC + IC + PI-Trim	20.6	57.13	948.21	1220.57	3.24
WC + IC + RL-Trim	20.6	58.81	965.47	1326.49	0.30

agent observes current, 2-, 4-, and 6-hour look-ahead values of T_{out} and $\hat{T}_i$, a 24-hour moving average of T_{out}, current values of T_i, $\dot{T}_i$, T_s, and T_r', and two time-of-day features. The reinforcement learning (RL) reward penalizes comfort violations, heat use, infeasible setpoints, and abrupt setpoint changes:

$$r_t = -500 d_t \left(1 + 2.4 d_t^2\right) - 2.4\dot{Q}_t - \left|\hat{T}'_{s,t} - T'_{s,t}\right| - 6\Delta a_t, \quad (9)$$

where d_t denotes the instantaneous comfort-violation severity and $\Delta a_t = |a_t - a_{t-1}|$. We remark that Eq. (9) does not directly penalize e.g. cumulative or peak mass flow, as this experiment is intended to demonstrate that the simulator allows for RL training rather than providing a deployment-ready control policy. Here, both actor and critic networks are multilayer perceptrons trained for 7×10^5 interaction steps. The agent is trained using data from D1 over the period from August 1, 2025 to February 27, 2026. All control strategies are then evaluated on the subsequent unseen period from February 28, 2026 to May 18, 2026, which serves as the validation period for the controller comparison.

RESULTS AND DISCUSSION

After calibration, the identified model parameters are reported in Table 1, and validation results are shown in Fig. 3. The fitted effectiveness reaches the imposed upper bound, $\epsilon = 1$, which is adopted as an effective approximation in the simulations. The identified radiator parameters should be interpreted as effective aggregate quantities. Because, calibration is based on secondary-side temperatures and $\bar{T}$, while the apartment-level number and placement of radiators, their characteristics, and complete DHW separation (c.f. Eq. (1)) are not available. Consequently, the fitted radiator model should be viewed as an aggregate representation of heat transfer to the indoor air mass.

The calibrated RC parameters cannot be directly mapped to physical properties of the building envelope, since multiple parameter combinations may yield similar values of Eq. (6) and several physical effects are represented through lumped states. Qualitatively, the fitted parameters indicate faster heat transfer through ventilation and internal thermal pathways than through the outer wall envelope, while the wall states exhibit substantially higher thermal storage capacity than the indoor air node. Despite its simplicity, the 4R3C model achieves a MAE of 5.8 kW and $R^2 = 0.78$ while remaining discrepancies are partly attributed to incomplete DHW load separation and the use of static values for ΔT_{DHW} and α. In comparison, the 3R2C model achieves an MAE of 5.83 kW and $R^2 = 0.77$, while repeated timing measurements on the same computing platform indicate an approximately 29% reduction in the RC-model runtime per time step. Although this advocates for simpler topologies, no measurable runtime reduction is observed when benchmarking the complete simulation loop, whose cost is not dominated by the RC state update. We therefore retain the 4R3C topology in the present study, while future work should address computational bottlenecks in the overall simulator.

The simulated night-setback control approaches are summarized in Table 2. For $\hat{T}_i = 21°\mathrm{C}$, indoor compensation substantially reduces comfort violations relative to the weather-compensation baseline. Adding a PI trim further reduces heat use at the expense of a modest increase in comfort violations. Lower daytime setpoints (20.8°C and 20.6°C) reduce heat use further, but increase comfort violations, as neither the indoor-compensation curve nor the PI trim explicitly accounts for the time-varying comfort bands. Because PI control is reactive, heat supply tends to increase immediately before and after the morning transition, reducing the benefit of a night setback and this contributes to a larger peak mass flow. When SAC trimming is applied, the comfort severity S is the lowest among all evaluated approaches. However, heat use, pumped mass, and peak mass flow remain comparable to, or higher than, those obtained using PI trimming. We reiterate that this is due to the fact that Eq. (9) penalizes the latter only indirectly such that comfort is prioritized over energy-related objectives. Consequently, the SAC results should be interpreted as a demonstration of RL training and evaluation within the simulator, rather than evidence of a deployment-ready controller.

CONCLUSIONS AND FUTURE WORK

This work presented and calibrated a lightweight grey-box simulator for district-heated residential buildings using op-

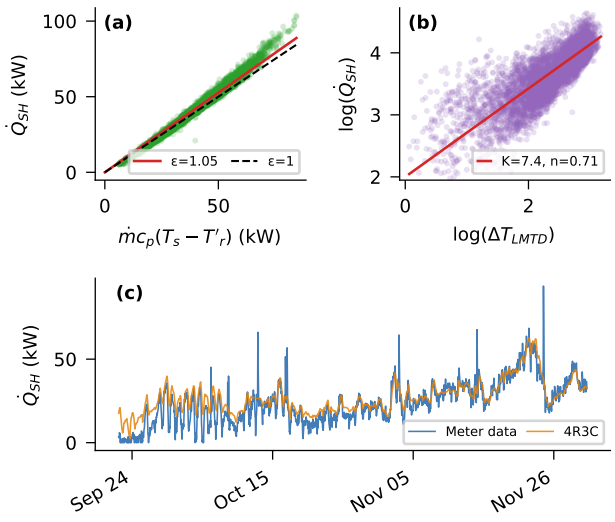

Figure 3: Calibration and Validation Results for the Coupled Substation–Building Model

erational measurements from a real building. The resulting simulator provides a computationally efficient aggregate representation of substation, radiator, and building envelope dynamics and was used to evaluate control strategies for heat savings under comfort constraints. The results indicate that rule-based control can maintain stable indoor temperatures, while PI-based setpoint trimming further reduces heat use with comparable comfort performance. The simulator also provides a platform for training and evaluating reinforcement learning controllers. Future work will focus on improving model fidelity through additional disturbance and occupancy modeling, incorporating an explicit DHW representation, and study alternative reward formulations that explicitly account for peak demand and cumulative mass flow.

ACKNOWLEDGEMENTS

This work was supported by the KKS DAS programme (Grant ID. 20230101) at the University of Borås. We express gratitude towards our anonymised network operator and facility-owner partners for data access and feedback.

REFERENCES

Boodi A.; Beddiar K.; Amirat Y.; and Benbouzid M., 2022. *Building thermal-network models: a comparative analysis, recommendations, and perspectives*. *Energies*, 15, no. 4, 1328.

Chaudhry A.; Lezaun N.; Fontes F.; and Bram S., 2021. *Model Predictive Control of a Substation of a District Heating System for Enhanced Environmental and Economic Performance*. In *International Conference on Applied Energy*. Bangkok, Thailand, 1–6.

Dolinay V. and Vasek L., 2019. *Benefits of night temperature setback in the control strategy of the district heating system*. In *MATEC Web of Conferences*. EDP Sciences, vol. 292, 01052.

Haarnoja T.; Zhou A.; Abbeel P.; and Levine S., 2018. *Soft actor-critic: Off-policy maximum entropy deep reinforcement learning with a stochastic actor*. In *International conference on machine learning*. Pmlr, 1861–1870.

International Energy Agency, 2025. *Energy Efficiency 2025*. Tech. rep., IEA, Paris. URL `https://www.iea.org/reports/energy-efficiency-2025`. Licence: CC BY 4.0.

Lienhard IV J.H. and Lienhard V J.H., 2019. *A Heat Transfer Textbook*. Dover Publications, Mineola, NY, 5th ed. ISBN 9780486837352. URL `https://ahtt.mit.edu`.

Lundström L. and Akander J., 2019. *Bayesian calibration with augmented stochastic state-space models of district-heated multifamily buildings*. *Energies*, 13, no. 1, 76.

Mathiesen B.; Gonzalo E.; Georgati M.; Nielsen S.; and Nikolic J., 2026. *Heat Roadmap Europe: Towards a sustainable, resilient and competitive heating sector by 2050 – Main report*. Aalborg Universitet, Denmark. ISBN 978-87-93541-63-4.

Muniak D.P., 2017. *Radiators in hydronic heating installations*. Springer.

Rodrigues R.; Pietzcker R.; Sitarz J.; Merfort A.; Hasse R.; Hoppe J.; Pehl M.; Ershad A.M.; Muessel J.; Schreyer F.; et al., 2026. *2040 greenhouse gas reduction targets and energy transitions in line with the EU Green Deal*. *Nature Communications*, 17, no. 1, 3417.

Sleptsov A.; Crisostomi E.; and Bischi A., 2021. *Control schemes for district heating substations considering user-defined building's indoor temperature*. *Building and Environment*, 191, 107598.

Wang X.; Ye Y.; Deng W.; Wu Y.; Zhang Z.; Wu T.; and Ma Y., 2026. *An adaptive grey-box model for nearly zero energy building operations in challenging climate*. *Energy*, 141151.

Zhang Z.; Zhou X.; Du H.; and Cui P., 2023. *A new model predictive control approach integrating physical and data-driven modelling for improved energy performance of district heating substations*. *Energy and Buildings*, 301, 113688.